CERN-TH.5670/90
FTUAM/08-90

The Role of Chiral Lagrangians in Strongly Interacting $W_L W_L$ Signals at pp Supercolliders

Antonio DOBADO[1]

Maria J. HERRERO[2]

CERN, CH-1211 Geneva, Switzerland

and

Juan TERRON

Departamento de Fisica Teorica de la Universidad
Autonoma de Madrid, 28049 Madrid, Spain

ABSTRACT

In this paper we apply a simple phenomenological model to describe the scattering amplitudes of strongly interacting longitudinal gauge bosons at the future pp colliders, LHC and SSC. The model is based on the use of the well-known techniques from chiral effective Lagrangians and chiral perturbation theory, supplemented by a unitarization method for the scattering amplitudes. The generality of the approach allows one to deal with various physical situations in the unknown symmetry breaking sector of the Standard Model. In particular we mimic the two typical scenarios for the symmetry breaking sector: one of Higgs-type and the other of QCD-type. Two different unitarization methods have been implemented for comparison: the Padé approximants method and the K-matrix method. The first one permits the incorporation of the possibility of dynamical resonances as it can develop poles for the various different (I,J)-channels. A systematic study of strongly interacting signals for both LHC and SSC is presented, and their rates and efficiencies are compared. The LHC project with the high luminosity option turns out to give quite promising results.

---

[1] On leave of absence from Departamento de Fisica Teorica de la Universidad Complutense de Madrid, 28040 Madrid, Spain

[2] On leave of absence from Departamento de Fisica Teorica de la Universidad Autonoma de Madrid, 28049 Madrid, Spain

CERN-TH.5670/90
FTUAM/08-90
February 1990

1 Introduction

The fact that the mass of the Higgs scalar M_H and the strength of the scalar self-coupling λ are not predicted in the Standard Model (SM) of electroweak interactions is essentially a manifestation of our ignorance about the dynamics triggering the spontaneous breakdown of the $SU(2)_L \times U(1)_Y$ gauge symmetry down to $U(1)_{em}$. The minimal Higgs sector of the SM is not even unique in the sense that it could be replaced by another physical system, not necessarily a system of fundamental scalar fields, that can reproduce the same pattern of the symmetry breaking mechanism. Generally speaking, all we need is an interacting symmetry breaking sector (SBS) that can provide at least three Goldstone bosons to become the longitudinal gauge boson modes (LWB) $W_L^{\pm}$ and Z_L. Furthermore, this SBS could be either a weakly or a strongly interacting physical system giving rise to very different phenomenological consequences.

Several arguments lead to the general conclusion that, no matter what the specific system for the SBS may be, some manifestation of it must appear at or below the TeV energy domain. In particular, if the SBS is weakly interacting there are typically a few light modes in the low energy spectrum, say much below 1 TeV. Two examples are the minimal SM with one light Higgs boson and the minimal supersymmetric version of the SM with two doublets of complex scalar fields. In contrast, the models with strongly interacting SBS (for instance, the SM with $M_H \geq 1TeV$ and models with dynamical symmetry breaking such as technicolour, composite models etc.) are characterized by the absence of light modes and the resonances typically belong to the few TeV energy region. Unfortunately, there is still no satisfactory working model for the strongly interacting SBS case with dynamical symmetry breaking that can account for the masses of all known particles without running into trouble with experimental facts.

The main purpose of this paper is to study, in a model-independent way, the most remarkable physical consequences of a strongly interacting SBS at the future proton-proton supercolliders, LHC and SSC. By model-independent way we mean without making any specific assumption "a priori" about the particular dynamics governing the SBS. For us and for the rest of this note, the strongly interacting SBS hypothesis simply means the absence of any physical state belonging to the SBS below about 1 TeV other than the LWB themselves. In that case, the relative low mass of the gauge bosons as compared to the TeV energy domain, where the emerging resonances are expected to occur, may be understood on the basis of an approximate global symmetry of the SBS which is spontaneously broken. As will be discussed later on, the simplest choice for the symmetry breakdown that encompasses the global symmetries of the SM and incorporates the so-called custodial symmetry as a reliable symmetry of the SBS, is given by the symmetry breaking pattern: $SU(2)_L \times SU(2)_R \to SU(2)_{L+R}$. The LWB are identified as the Goldstone bosons associated to this symmetry breaking, and this is why they are light when compared with the TeV scale.

The precise relation between the longitudinal modes and the Goldstone bosons is given by the equivalence theorem [1]. This theorem states that for energies $\sqrt{s}$ much greater than M_W, the scattering amplitude for any process involving LWB is approximately equal (up to corrections of the order of $M_W/\sqrt{s}$) to the amplitude for the same process with the LWB , W_L^i, replaced by the corresponding Goldstone bosons, w^i. That is,

$$M(W_L^i(p_1), W_L^j(p_2), ...) = M(w^i(p_1), w^j(p_2), ...) + O(\tfrac{M_W}{\sqrt{s}}).$$

The key point is that when the SBS is strongly interacting, the self-coupling of the Goldstone bosons becomes large and, therefore, their scattering amplitudes also become large. By means of the equivalence theorem at energies $\sqrt{s} \gg M_W$, one concludes then that the scattering amplitudes of the LWB, $W_L^i W_L^j \to W_L^k W_L^l$, are large and dominant with respect to other scattering processes involving $W's$ and $Z's$ that are typically governed by the weak coupling constant. This last fact leads to the central idea that by measuring the number of gauge boson pairs produced through the WW fusion mechanism (fig.1) at high enough energies (say around the TeV energy scale) we are measuring the strength of the interactions in the SBS. In particular, WW fusion will provide a significant enhanced rate of LWB pairs if and only if the SBS is strongly interacting.

The subject of $W_L W_L$ production at TeV energies has been largely discussed in the literature in the context of heavy Higgs boson production by WW fusion at supercolliders [2]. It has also been considered in a more general context of strongly interacting LWB by Chanowitz and Gaillard in [1]. The essential point in their study is the use of the so-called " Low Energy Theorems" (LET) [3] in order to evaluate the scattering amplitudes for the LWB that can be applied to make an estimate of the expected rates in $W_L W_L$ production at TeV energies. In particular it has been studied in more detail the rates for the SSC [4]. The LET, however, do not distinguish among the different possible underlying SBS dynamics that, certainly, would give different patterns in the $W_L W_L$ scattering amplitudes. The analogy in QCD is provided by the well-known $\pi\pi$ scattering amplitudes or pion-LET results of Weinberg [5]. One example is $M(\pi^+\pi^- \to \pi^0\pi^0) = \frac{s}{f^2}$. These amplitudes show no dependence on the underlying theory, and only when the next contributing terms in the low energy expansion are taken into account is it possible to recognize the low energy remainder of QCD.

Motivated by the idea that the behaviour of the $W_L W_L$ scattering amplitudes at TeV energies can provide the answer to the enigma of the SBS and the type of dynamics underlying it, we developed in a previous work [6] a phenomenologically viable model for these amplitudes, based on a chiral Lagrangian approach to order p^4, with p being the typical momentum scale of the external LWB. Since the theory of effective chiral Lagrangians provides a compact and elegant method for dealing with the interactions of the Goldstone modes of any theory, even in the case where the underlying dynamics is not known, we believe it is the most appropriate approach to the problem of strongly interacting LWB [7]. The model of ref.[6] was built up from the simplest choice for the symmetry breaking

pattern , $SU(2)_L \times SU(2)_R \to SU(2)_{L+R}$, and, within the chiral perturbation theory approach, it is renormalizable up to order p^4. At order p^2 it reproduces the LET results and, to next order $O(p^4)$, the one-loop scattering amplitudes show a dependence on two new unknown parameters that represent in a generic way the dependence on the underlying unknown dynamics. Different theories will give different values for these parameters and ultimately it should be possible to obtain them as a prediction from the real theory. It could well happen that by the time the relevant experiments like SSC, LHC and CLIC start working the real theory will still be unknown. However, even in that case, the parameters could be obtained phenomenologically and from them we could learn, hopefully, about the underlying theory.

In this paper we have carried out a systematic study of strongly interacting LWB signals at future LHC and SSC colliders by applying the model of ref.[6]. In particular we mimic with this model two different scenarios for the SBS that we tentatively call Higgs-like and QCD-like models respectively. We have also included two different procedures to unitarize the scattering amplitudes, namely, the Padé approximants approach and the K-matrix method. As they both fulfil exactly elastic unitarity at all energies, they can be used to make reasonable predictions for the next generation colliders that will scan into the TeV energy domain.

In view of the growing interest concerning the recent proposal of a high luminosity option for the LHC project [8] we have performed the whole analysis in parallel for both LHC and SSC. It will allow us to compare them as far as efficiency in detecting the strongly interacting LWB signals is concerned. As we shall see, the outcome turns out to be quite satisfactory for the case of the LHC machine with the high luminosity option.

The paper is organized as follows. Section 2 is a review of the model presented in [6]. Section 3 is devoted to the unitarization procedures of the partial wave amplitudes that are obtained from the model described in sec.2. In section 4 we present the analytical formulae for the computation of the cross-sections corresponding to the strongly interacting LWB signals at pp supercolliders. Section 5 is dedicated to the calculation of the cross-sections for the background processes. Section 6 contains all the numerical results for the signal and background rates at SSC and LHC. In sec.6 is also described the optimization procedure that was used in order to find the most efficient cuts in separating the signal from the background. The conclusion of this work is outlined in section 7.

2 The model for the LWB scattering amplitudes

In this section we shall review the chiral Lagrangian description of ref.[6] for the scattering amplitudes of the LWB which should apply in the case of these modes being strongly interacting.

As has been anticipated in the introduction, we shall assume that the only physical states belonging to the SBS at low energies (compared with the mass of the lightest resonance) are the LWB. Let us think of these modes as the Goldstone bosons associated to the spontaneous symmetry breaking of a (approximate) global symmetry of the SBS, G, down to a lesser symmetry $H \subset G$. Although we do not know which groups are G and H, gauge invariance of the SM restricts them to those satisfying $G \supset SU(2)_L \times U(1)_Y$ and $H \supset U(1)_{em}$. Since we have assumed that there are no other Goldstone or pseudo-Goldstone bosons in the low energy spectrum, then two possibilities follow: either (1) $G = SU(2)_L \times SU(2)_R$, $H = SU(2)_{L+R}$, or (2) $G = SU(2)_L \times U(1)_Y$, $H = U(1)_{em}$. The residual group $SU(2)_{L+R}$ in the first case is called the custodial symmetry group because it has the important role of guaranteeing the value of the ratio $\rho = \frac{M_W^2}{M_Z^2 cos^2\theta_W}$ to be equal to one, in close agreement with the experimental value $\rho_{exp} = 1.01 \pm 0.01$ [9]. Incidentally, the additional chiral symmetry $SU(2)_L \times SU(2)_R$ is, in fact, a global symmetry in the simplest scenario for the SBS of the SM with just one $SU(2)_L$ doublet of complex scalar fields.

In the following we will adopt the first symmetry breaking pattern, namely,

$$SU(2)_L \times SU(2)_R \to SU(2)_{L+R} \tag{2.1}$$

and will assume $\rho = 1$ for all what rests. It is worth to recall that this chiral symmetry (as well as the custodial symmetry) gets explicitly broken once the global subgroup $SU(2)_L \times U(1)_Y$ is gauged by terms proportional to g', the $U(1)_Y$ coupling constant. However, we will not consider here explicit chiral breaking terms. Since our main interest is the study of the most remarkable strongly interacting LWB signals, we will work within the approximation of neglecting the interactions of electroweak strength, that is, we will take $g, g' = 0$. In other words, we will not consider the coupling of the LWB to the transverse modes nor the photon.

In order to obtain the LWB scattering amplitudes we have followed closely the phenomenological chiral Lagrangian approach proposed in an early work by Weinberg [10]. This method has become very useful in describing in a systematic way the low energy structure of strong interactions among pseudoscalar mesons [11].

The starting point is the use of a convenient parametrization for the Goldstone boson fields $w_1(x), w_2(x), w_3(x)$ associated to the symmetry breaking $SU(2)_L \times SU(2)_R \to SU(2)_{L+R}$. This parametrization is given in terms of a unitary matrix field $U(x)$ belonging to the quotient space $SU(2)_L \times SU(2)_R / SU(2)_{L+R}$ and is defined by:

$$U(x) = exp(\frac{i}{v} w_a(x)\sigma^a) \tag{2.2}$$

with $\sigma^a, a = 1, 2, 3$ being the Pauli matrices, and v is fixed experimentally by the Fermi constant to the value $v = (G_F\sqrt{2})^{-1/2} = 246 GeV$.

Under a chiral $SU(2)_L \times SU(2)_R$ transformation the $U(x)$ matrix field transforms as:

$$U(x) \to V_L U(x) V_R^+ \tag{2.3}$$

with $U_L \in SU(2)_L$ and $U_R \in SU(2)_R$.

The most general chiral invariant Lagrangian is a sum of infinite terms with increasing (even) number of derivatives in the $U(x)$ and the $U(x)^+$ fields and with an infinite number of arbitrary parameters. The resulting effective theory of interacting Goldstone bosons from this general Lagrangian is renormalizable in the sense that all the counterterms needed to remove the infinities appearing in the Green functions from loop contributions are already present in the original Lagrangian. The whole point of an expansion in terms of an increasing number of derivatives, or equivalently in terms of increasing powers of the external momenta, is that at low energy only a finite number of terms are important. Here low energy means much lower than the typical parameter scale that controls the chiral expansion of about $1\pi v$ [12]. It follows then that keeping just a few terms in the chiral Lagrangian makes sense and the model can be used to parametrize in a consistent way the low energy scattering amplitudes as a function of a finite number of parameters. To a given order in the chiral expansion the inclusion of loop diagrams will generate a scale dependence that is reabsorbed into the definition of the renormalized parameters while the physical amplitudes remain scale independent. The framework just outlined above is well known in the context of scalar meson interactions, and is commonly referred to in the literature as chiral perturbation theory (ChPT). Our goal is precisely to parametrize the presumably measurable scattering amplitudes for the LWB in terms of these phenomenological parameters.

To lowest order in ChPT, $O(p^2)$, the chiral Lagrangian is fixed in terms of just one parameter, v, and has the form:

$$\mathcal{L}_0 = \frac{v^2}{4} Tr(\partial_\mu U \partial^\mu U^+). \tag{2.4}$$

To next-to-leading order, $O(p^4)$, two additional terms have to be included which can be written in the form:

$$\mathcal{L}_1 = MTr(\partial_\mu U \partial^\mu U^+) Tr(\partial_\nu U \partial^\nu U^+) + NTr(\partial_\mu U \partial_\nu U^+) Tr(\partial^\mu U \partial^\nu U^+), \tag{2.5}$$

with M and N being two dimensionless parameters.

The predictions for the Goldstone boson interactions (or, equivalently, for the LWB) to lowest order are those of $\mathcal{L}_0$ and therefore depend just on v. They lead to the well-known LET results for the Goldstone boson scattering amplitudes, $T^{LET}(w_i w_j \to w_k w_l) \equiv T^{LET}_{ijkl}$ with $i,j,k,l = 1,2,3$. In terms of the standard basis for the Goldstone bosons, $w^\pm = \frac{1}{\sqrt{2}}(w_1 \mp w_2)$ and $z^0 = w_3$, they are given by:

$$T^{LET}_{+-+-} = -\frac{u}{v^2}\ ,\ T^{LET}_{+-00} = \frac{s}{v^2}\ ,\ T^{LET}_{0000} = 0. \tag{2.6}$$

For next order predictions, $O(p^4)$, we use $\mathcal{L} = \mathcal{L}_0 + \mathcal{L}_1$ instead of $\mathcal{L}_0$ and include the one-loop corrections to $\mathcal{L}_0$ that are also of order $O(p^4)$. The explicit formulae for the

amplitudes were obtained in [6] by using the dimensional regularization scheme. They were in agreement with the early results by Weinberg [10] and by Gasser and Leutwyler [11] for the $\pi - \pi$ scattering amplitudes to order $O(p^4)$ in the chiral limit.

The Goldstone boson amplitudes to $O(p^4)$ are given by:

$$T_{ijkl} = T^{LET}_{ijkl} + T^{(4)}_{ijkl}, \tag{2.7}$$

where T^{LET}_{ijkl} are those of eq.(2.6) and $T^{(4)}_{ijkl}$ are given as follows (here the superscript (4) refers to the $O(p^4)$ contributions):

$$T^{(4)}_{+-+-} = \frac{4}{v^4}(2M_R(\nu)(s^2+t^2) + N_R(\nu)(s^2+t^2+2u^2))$$
$$+\frac{4}{(4\pi)^2 v^4}[\frac{-1}{12}(9s^2+u^2-t^2)\log\frac{-s}{\nu^2} - \frac{1}{12}(9t^2+u^2-s^2)\log\frac{-t}{\nu^2} - \frac{1}{2}u^2\log\frac{-u}{\nu^2}]$$

$$T^{(4)}_{0000} = \frac{8}{v^4}(M_R(\nu)+N_R(\nu))(s^2+t^2+u^2)$$
$$+\frac{4}{(4\pi)^2 v^4}[-s^2\log\frac{-s}{\nu^2} - t^2\log\frac{-t}{\nu^2} - u^2\log\frac{-u}{\nu^2}]$$

$$T^{(4)}_{+-00} = \frac{4}{v^4}(2M_R(\nu)s^2 + N_R(\nu)(t^2+u^2))$$
$$+\frac{4}{(4\pi)^2 v^4}[-\frac{1}{12}(3t^2+u^2-s^2)\log\frac{-t}{\nu^2} - \frac{1}{12}(3u^2+t^2-s^2)\log\frac{-u}{\nu^2} - \frac{1}{2}s^2\log\frac{-s}{\nu^2}], \tag{2.8}$$

and, by the use of crossing symmetry, any other amplitude can be related to these three independent ones above.

The renormalized constants M_R and N_R are defined in terms of the bare ones M and N so as to cancel the divergences appearing because of the one-loop corrections to $\mathcal{L}_0$. It introduces a dependence of M_R and N_R on the renormalization scale parameter ν that can be easily fixed by demanding the physical amplitudes T_{ijkl} to be independent of this scale parameter, i.e., $\frac{dT_{ijkl}}{d\nu} = 0$. This gives:

$$M_R(\nu) = M_R(\nu_0) - \frac{1}{12(4\pi)^2}\log\frac{\nu}{\nu_0}$$
$$N_R(\nu) = N_R(\nu_0) - \frac{1}{6(4\pi)^2}\log\frac{\nu}{\nu_0}, \tag{2.9}$$

where ν_0 is again a reference scale which cannot be set to zero.

The amplitudes $T^{(4)}$ can be interpreted as follows. The polynomial terms in s,t and u variables, proportional to M_R and N_R, are the same that would have been obtained at the tree level from $\mathcal{L}_1$ with the substitution of the renormalized parameters by the bare ones. The effect of the one-loop corrections to $\mathcal{L}_0$ is explicitly shown in the amplitudes by the

appearance of new logarithmic terms and the scale dependence in the renormalized parameters commented above. The model in this form is completely meaningful and depends on two unknown parameters, M_R and N_R, which contain the information relative to the underlying dynamics. The only thing to bear in mind is that the eventual measurement of these parameters will have to be accompanied by the value of the scale ν at which they have been defined. The value of the M_R and N_R at any other energy scale ν' then can be obtained by the use of eq. (2.9).

So far, all that has been said is completely general and can be applied irrespective of the underlying theory. The important outcome to learn is that different choices of M_R and N_R at an arbitrary scale ν will describe different physical situations in the symmetry breaking sector of the SM. For the purpose of this paper we have chosen in particular to mimic two typical examples, namely, the minimal SM with a very heavy scalar Higgs ($M_H > 1TeV$) and a scaled-QCD within the spirit of technicolour models. For us, they are somehow representative of a set of theories with a low energy behaviour governed respectively by the existence of either a scalar resonance ("scalar-dominated theories") or a vector resonance ("vector-dominated theories") in the TeV energy spectrum. In the following we will refer to them as Higgs-like and QCD-like models respectively.

Higgs-like model:

In order to mimic the minimal SM with a very heavy scalar Higgs by means of the chiral Lagrangian approach, we have used the results for the LWB scattering amplitudes that have been obtained recently at the one-loop level and in the framework of the renormalizable SM in [13] and independently in [14]. By comparing our results of eqs.(2.6),(2.7) and (2.8) with the results given in refs.[13] and [14] in the limit $M_H^2 \gg s$, one may immediately conclude that the chiral Lagrangian approach reproduces the one-loop LWB scattering amplitudes of the SM, provided the renormalized parameters $M_R(\nu)$ and $N_R(\nu)$ are defined in terms of M_H as follows:

$$M_R(\nu) = \frac{1}{8}(c_1 - \frac{1}{2}c_2) + \frac{1}{12(4\pi)^2} log \frac{M_H}{\nu}$$

$$N_R(\nu) = \frac{c_2}{8} + \frac{1}{6(4\pi)^2} log \frac{M_H}{\nu} \qquad (2.10)$$

where

$$c_1 = \frac{1}{(4\pi)^2}(\frac{9\pi}{2\sqrt{3}} - \frac{76}{9}), \quad c_2 = -\frac{1}{9}\frac{1}{(4\pi)^2} \qquad (2.11)$$

and M_H is the renormalized Higgs mass as defined in ref.[13]. More precisely, M_H is set by the equation:

$$M_H^2 = 2\lambda(M_H)v^2 \qquad (2.12)$$

where $\lambda(\nu)$ is the well-known renormalized coupling constant to one loop:

$$\lambda(\nu) = \frac{\lambda(M_H)}{1 - \frac{3\lambda(M_H)}{2\pi^2} log \frac{\nu}{M_H}}. \qquad (2.13)$$

A few comments are in order. First of all it is important to have in mind that our comparison with the results of the SM only applies in the limit of a large (finite) renormalized Higgs mass parameter, $s \ll M_H^2$. As already emphasized in ref.[13], in this limit the one-loop amplitude is of order $\frac{s}{(4\pi v)^2}$ with respect to the tree amplitude, where s symbolizes s, t or u. This means that for $s \ll M_H^2$ the loop-expansion is not perturbative in $\lambda(M_H)$ as it corresponds to an expansion in powers of $\frac{s}{(4\pi v)^2}$ rather than $\frac{\lambda(M_H)}{4\pi}$. Secondly, in the large M_H limit we do not expect M_H to be the mass of a physical particle or resonance. Equivalently, we do not expect M_H to coincide with the position of a pole in the (exact) Green functions of the strongly interacting theory. In practice a physical scalar resonance of Higgs type (with the same quantum numbers) would manifest as a pole in the second Riemann sheet of the $I = J = 0$ channel for the LWB scattering amplitudes, and, in general, the physical mass of the scalar resonance, M_S, will not coincide with the renormalized Higgs mass M_H [15].

QCD-like model:

In order to mimic a QCD-like scenario for the SBS of the SM we have simply assumed a pattern for the Goldstone boson scattering amplitudes $M(w_i w_j \to w_k w_l)$ similar to that of the pion-pion scattering amplitudes, $M(\pi_i \pi_j \to \pi_k \pi_l)$, but with the energy conveniently scaled by a factor $\alpha = \frac{v}{f_\pi}$, where $f_\pi = 0.0916eV$ is the pion decay constant, and $v = 246GeV$. This is equivalent to assuming that the underlying theory governing the SBS of the SM is similar to QCD (it would correspond ,therefore, to a technicolour theory with a number of technicolours $N_{TC} = 3$) and hence it is reasonable to use a similar low-energy approach for the Goldstone bosons of the two theories. In the language of the chiral Lagrangian approach, it corresponds to taking the same numerical values for the parameters M_R and N_R as the ones that, presumably, should be predicted from QCD but referred to a scale $\nu'(GeV) = \alpha\ \nu(GeV)$ instead of the scale ν. In view of the lack of a clear prediction from QCD for M_R and N_R we will instead use for them the values that fit the pion-pion scattering data better. Let us call these values $M_R^{exp}(\nu)$ and $N_R^{exp}(\nu)$ respectively. Thus, we define the values of M_R and N_R at ν' for the scaled QCD- model as:

$$M_R(\alpha\ \nu\ GeV) = M_R^{exp}(\nu\ GeV)$$

$$N_R(\alpha\ \nu\ GeV) = N_R^{exp}(\nu\ GeV). \qquad (2.14)$$

For several attempts at getting M_R^{exp} and N_R^{exp} from the pion-pion experimental data, see refs.[16] and [17].

3 Partial waves and unitarization procedures

In this section we will deal with the subject of unitarity in the context of the model presented in sec.2. To start, let us write down the lowest partial wave amplitudes a_{IJ} ($I = 0, 1, 2\ ;\ J = 0, 1$) corresponding to the LWB scattering amplitudes given in eqs.(2.6),(2.7)

and (2.8). With the same notation as in sec.2, they are:

$$a_{IJ}(s) = a_{IJ}^{LET}(s) + a_{IJ}^{(1)}(s) \tag{3.1}$$

$$a_{00}^{LET}(s) = \frac{s}{16\pi v^2}\ ;\ a_{20}^{LET}(s) = -\frac{s}{32\pi v^2}\ ;\ a_{11}^{LET}(s) = \frac{s}{96\pi v^2} \tag{3.2}$$

$$a_{00}^{(4)} = \frac{s^2}{64\pi v^4}[\frac{1}{3}(176M_R(\nu) + 112N_R(\nu)) + \frac{1}{(4\pi)^2}(\frac{11}{27} - \frac{50}{9}log\frac{s}{\nu^2} + 1i\pi)]$$

$$a_{20}^{(4)} = \frac{s^2}{64\pi v^4}[\frac{32}{3}(M_R(\nu) + 2N_R(\nu)) + \frac{1}{(4\pi)^2}(\frac{25}{51} - \frac{20}{9}log\frac{s}{\nu^2} + i\pi)]$$

$$a_{11}^{(4)} = \frac{s^2}{96\pi v^4}[4(-2M_R(\nu) + N_R(\nu)) + \frac{1}{(4\pi)^2}(-\frac{1}{18} + i\frac{\pi}{6})]$$

$$a_{01}(s) = a_{21}(s) = 0. \tag{3.3}$$

It is obvious that the LET predictions for the partial wave amplitudes, eq.(3.2), cannot fulfil the basic requirement of elastic unitarity at any energy. This is simply because all the $a_{IJ}^{LET}(s)$ are real whereas the elastic unitarity condition in terms of the partial wave amplitudes reads:

$$Im\ a_{IJ}(s) = |a_{IJ}(s)|^2. \tag{3.4}$$

However, the one-loop partial wave amplitudes of eq.(3.1) have a much better unitarity behaviour, since, as can be easily checked, they fulfil instead:

$$Im\ a_{IJ}(s) = Im\ a_{IJ}^{(4)}(s) = |a_{IJ}^{LET}(s)|^2. \tag{3.5}$$

This means they are perturbatively (in the sense of ChPT) unitary and, therefore, they are approximately unitary just at low energies. In fact, in ref.[6] it was shown that for the models of interest here exact (elastic) unitarity, eq.(3.4), is badly violated for energies above about 1.5 TeV. Unfortunately, it is a problem one has to deal with, since after all we are interested in applying the model to make predictions for pp machines that will scan subprocess energies in the TeV domain.

In order to extend the range of applicability of the model in sec.2 we have unitarized the partial wave amplitudes of eq.(3.1) by two different methods. These are: the use of the Padé approximants for the partial wave amplitudes (see for instance [18]) and the K-matrix method (see for instance [19]). The K-matrix method produces a unitary output by starting from an expansion for the S-matrix that in general is not unitary order by order in the expansion. It has been used previously in the context of strongly interacting LWB by several authors. For instance, it was used in [20] to unitarize the LET results and in [21] to unitarize the one-loop results of [13].

Following the notation of eq.(3.1), the K-matrix method is equivalent to define the unitarized partial wave amplitudes as follows:

$$a_{IJ}^{K}(s) \equiv \frac{a_{IJ}^{LET}(s) + Re\ a_{IJ}^{(4)}(s)}{1 - i(a_{IJ}^{LET}(s) + Re\ a_{IJ}^{(1)}(s))}. \tag{3.6}$$

They verify at any energy

$$Im\ a_{IJ}^{K}(s) = |a_{IJ}^{K}(s)|^2, \tag{3.7}$$

and for low energies they behave as

$$a_{IJ}^{K}(s) = a_{IJ}(s) + O(s^3), \tag{3.8}$$

provided eq.(3.5) holds.

The Padé method has also been used previously in the context of strongly interacting LWB by a number of authors (see for instance refs.[15] and [20]). In the different context of low energy meson physics, the application of this method in order to unitarize the pion-pion scattering amplitudes, as predicted in ChPT to one loop has given quite satisfactory results and the agreement with the experimental data is excellent [17].

For the purpose of this paper, the relevant Padé approximants for the partial wave amplitudes are the $[1,1]$ ones which in the notation of eq.(3.1) are defined as follows,

$$a_{IJ}^{[1,1]}(s) \equiv \frac{a_{IJ}^{LET}(s)}{1 - \frac{a_{IJ}^{(4)}(s)}{a_{IJ}^{LET}(s)}}. \tag{3.9}$$

At low energies, they behave as

$$a_{IJ}^{[1,1]}(s) = a_{IJ}(s) + O(s^3) \tag{3.10}$$

and at any energy they verify

$$Im\ a_{IJ}^{[1,1]}(s) = |a_{IJ}^{[1,1]}(s)|^2, \tag{3.11}$$

provided eq.(3.5) holds.

Futhermore, the $a_{IJ}^{[1,1]}(s)$ have the same structure of cuts in the s-complex plane as the one-loop results of ChPT, $a_{IJ}(s)$. In addition it offers the interesting possibility of incorporating resonances since it can develop poles in the second Riemann sheet for the various different (I,J) channels [15]. This last property is always desirable in strongly interacting theories where a rich spectrum is expected to appear. In particular, for our case, a pole in the $I = J = 0$ channel could simulate a scalar resonance of Higgs-like type, a pole in the $I = J = 1$ channel could simulate a vector resonance of ρ-like type (the technirho of $SU(3)$ technicolour theories), etc..On the contrary, the K-matrix method does not generate such a resonant behaviour. This last method, however, turns out to be more appropriate for situations where the partial wave amplitudes have rather a saturation behaviour above a certain energy value.

In order to illustrate the different behaviours of the two unitarization procedures when applied to the amplitudes of eq.(3.1), we have plotted in figs.(2.a) to (2.f) the results for $|a_{IJ}^{K}(s)|^2$ (dashed lines) and $|a_{IJ}^{[1,1]}(s)|^2$ (dotted lines) as a function of the energy $\sqrt{s}$. We

have also included in the figures the non-unitarized amplitudes of eq.(3.1) for comparison (solid lines). In particular, it is interesting to compare the two unitarization methods in the context of the models under study here, the Higgs-like and the QCD-like models as defined in sec.2. In the QCD-like case we have chosen for M_R^{exp} and N_R^{exp} in eq.(2.11) the numerical values obtained in ref.[17] from the best fit to the pion-pion scattering data. Following the notation of ref.[17] these numerical values at $\nu = 0.785\ GeV$ are given by:

$$M_R^{exp}(0.785\ GeV) = \frac{1}{16}(2G_R^{exp}(0.785\ GeV) - F_R^{exp}(0.785\ GeV))$$

$$N_R^{exp}(0.785\ GeV) = \frac{1}{16}F_R^{exp}(0.785\ GeV) \qquad (3.12)$$

where

$$F_R^{exp}(0.785\ GeV) = 0.029\ ;\ G_R^{exp}(0.785\ GeV) = 0.0073.$$

Correspondingly, the values of the renormalized parameters in eq.(2.14) at the scale $\nu' = \frac{\pi}{f_\pi}0.785\ GeV = 2054\ GeV$ are the following:

$$M_R(2054\ GeV) = -0.0009\ ;\ N_R(2054\ GeV) = 0.0018. \qquad (3.13)$$

In the rest of this section we will make some comments about figs.(2.a) to (2.f).

Effectively, the K-matrix method gives (dashed lines) in all the cases a saturation behaviour. The [1,1] Padé approximant method (dotted lines) develops a resonance in the $I = J = 0$ channel for the Higgs-like model and a resonance in the $I = J = 1$ channel for the QCD-like model. From now on we will call these resonances the scalar-Higgs-like resonance, S, and vector-ρ-like resonance, V. The V-resonance shows up at about $M_V \sim 2TeV$, and is in concordance with what is expected in technicolour models with $N_{TC} = 3$. The appearance of this V-resonance is an inmediate consequence in the QCD-like model since there is a repetition of all the relevant facts of pion-pion scattering data at energies scaled by a factor $\frac{\pi}{f_\pi}$, for instance, a broad enhancement in the $I = J = 0$ channel, the appearance of the ρ-resonance in the $I = J = 1$ channel, etc..

The S-resonance of the Higgs-like model shows up at a mass scale which is given by the position of the pole in the unphysical sheet of the $a_{00}^{[1,1]}(s)$ function [15]. More precisely, M_S is given by the solution to the equation:

$$M_S^2 = \frac{4v^2}{\frac{1}{3}(22c_1 + \frac{1}{4}c_2) + \frac{100}{9(4\pi)^2}log\frac{M_H}{M_S}}, \qquad (3.14)$$

where c_1, c_2 and the renormalized Higgs mass M_H have been defined in eqs.(2.11),(2.12) and (2.13) respectively. Although the solution for M_S in eq.(3.14) depends on the precise value of M_H, with M_S decreasing for M_H increasing, however, as can be easily checked, M_S is a very slowly varying function of M_H, and stays around $1TeV$ for a quite broad range of M_H values (see A.Dobado in [15] for more details). For instance, for $M_H = 10, 20, 10^2, 10^3, 10^{16}\ TeV$ the corresponding solutions for M_S are $M_S = 1.39, 1.11, 0.87, 0.70, 0.30\ TeV$, and the value of M_H at which M_S crosses by $M_S = 1\ TeV$ is $M_H = 38\ TeV$. The appearance of this pole in $a_{00}^{[1,1]}(s)$ as a function of M_H is reflected in figs.(2.a), (2.b) and (2.c) (dotted lines) that correspond to taking $M_H = 20, 10$ and $5TeV$ respectively. For lower values than about $M_H = 10TeV$ (see for instance fig.(2.c) with $M_H = 5TeV$) there is no such resonance since the width becomes comparable or even higher than the mass. As we have emphasized in section 2, the model should not be applied for too low values of M_H since our LWB amplitudes for the Higgs-like model are based in the limit of $s \ll M_H^2$.

From fig.2, it is clear that for the cases where there is no resonant behaviour, both unitarization methods give a very similar result. See, for instance, figs.(2.c),(2.e) and (2.f). In particular, from figs.(2.a), (2.b) and (2.c) it is also clear that the $a_{00}^{[1,1]}$ amplitude approaches the a_{00}^K amplitude from above as M_H decreases, or, equivalently, as the resonance gets heavier and broader and tends to disappear. Thus, effectively, the two methods act as two limiting situations, each one providing alternatively an output that will be closer to reality depending on whether finally in Nature there is (Padé method), or there is not such a resonant behaviour (K-matrix method).

4 Cross-sections for strongly interacting LWB signals

In this section we will present the analytical formulas for the computation of the cross-sections for strongly interacting LWB signals at pp supercolliders via the so-called WW-fusion mechanism depicted generically in fig.(1). More specifically, we have concentrated on the case where the two final gauge bosons are ZZ bosons. In view of the recent results from CDF [22] for the lower limit on the top quark mass of $m_t > 77GeV$, already pretty close to M_W, the possibility that the top quark is, in fact, heavier than the W gauge boson is becoming more realistic. For the particular case of strongly interacting signals (as well as for heavy Higgs searches) this possibility would certainly be a serious problem as far as the searches in WW and WZ final states is concerned. The reason is that for $m_t > M_W$ the top quarks (those produced mainly by strong interactions) decay into real W's with (almost) a 100% branching ratio. Hence, it provides some additional WW and WZ background contributions (usually not taken into account in the existing literature on this subject) that overwhelm the signal. Thus, the safest choice in terms of the signal-to-background ratio is the ZZ final state.

In order to compute the cross-section for the process

$$pp \to (V_1^L V_2^L \to V_3^L V_4^L) + X,$$

we have used the effective W-approximation [23] that allows us to derive it in terms of the cross-section for the subprocess $V_1^L V_2^L \to V_3^L V_4^L$, where the initial LWB are taken to be real. More precisely, it is given by:

$$\sigma = \sum_{ij}\int\int d\tau d\eta f_i(x_1,Q^2) f_j(x_2,Q^2) \int\int d\hat{\tau} d\hat{\eta} (\frac{d^2\mathcal{L}}{d\hat{\tau} d\hat{\eta}})_{V_1^L V_2^L / q_i q_j} \int_{-1}^{1} dcos\theta \frac{d\hat{\sigma}}{dcos\theta}(V_1^L V_2^L \to V_3^L V_4^L) \qquad (4.1)$$

where
f_i and f_j are the distribution functions of the quarks i and j, respectively, inside the proton; the variables τ and η are related to the momentum fractions of the quarks by $x_{1,2} = \sqrt{\tau}e^{\pm\eta}$; $(\frac{d^2\mathcal{L}}{d\tau d\eta})$ is the luminosity function for the gauge boson pair $V_1^L V_2^L$ to be radiated from the quark pair $q_i q_j$; and $\frac{d\hat{\sigma}}{dcos\theta}$ is the differential cross-section for the subprocess $V_1^L V_2^L \to V_3^L V_4^L$.

The luminosity function is given by:

$$(\frac{d^2\mathcal{L}}{d\tau d\eta}) = \prod_{i=1,2} f_{V_i}\frac{1-x_i}{x_i}, \tag{1.2}$$

where the values of the f_{V_i}'s depend on the particular gauge boson V_i and also on the type of quark it comes from:

$$f_W = \frac{\alpha}{4\pi x_w}$$

$$f_{Z\ u\bar{u}} = \frac{\alpha}{16\pi x_w(1-x_w)}[1+(1-\frac{8}{3}x_w)^2]$$

$$f_{Z\to t\bar{t}} = \frac{\alpha}{16\pi x_w(1-x_w)}[1+(1-\frac{4}{3}x_w)^2]. \tag{1.3}$$

Here, $x_w = sin^2\theta_w$, α is the electromagnetic coupling constant, and, the variables $\hat{\tau}$ and $\hat{\eta}$ are related to the momentum fractions of V_1, V_2 respect to q_i, q_j, x_1 and x_2, by $\hat{x}_{1,2} = \sqrt{\hat{\tau}}e^{\pm\hat{\eta}}$.

The connection between the variables $\tau, \eta, \hat{\tau}, \hat{\eta}$ and the relevant variables for the experimental analysis of $V_L V_L$ strongly interacting signals, namely, the invariant mass of the $V_L V_L$ pair, M_{VV}, the rapidity of the final V_L's, $y_{1,2}$, the transverse momentum of the final V_L's, p_{TV}, and, the total pp energy, $\sqrt{s}$, is given by the well-known relations:

$$y_{1,2} = \eta + \hat{\eta} \pm \frac{1}{2}log(\frac{1+\beta_V cos\theta}{1-\beta_V cos\theta})\ ;\ \beta_V = \frac{|p_V|}{E_V}$$

$$p_{TV} = |p_V|sin\theta$$

$$\hat{\tau} = \frac{M_{VV}^2}{\tau s}. \tag{1.1}$$

The differential cross-section for the scattering subprocess $V_1^L V_2^L \to V_3^L V_4^L$ is given by:

$$\frac{d\hat{\sigma}}{dcos\theta} = \frac{|T(V_1^L V_2^L \to V_3^L V_4^L)|^2}{64\pi M_{VV}^2}, \tag{4.5}$$

where we have included a factor $\frac{1}{2}$ due to the identity of the final state particles.

In order to compute the scattering amplitudes for the subprocesses $T(V_1^L V_2^L \to V_3^L V_4^L) \equiv T_{ijkl}$, where $i,j,k,l = +,-,0$, we have used their expansion in terms of the partial wave amplitudes, namely,

$$T_{ijkl} = 32\pi \sum_{I,J} a_{IJ}(s_{VV})(2J+1)\mathcal{P}_J(cos\theta)P_{ijkl}^I \tag{1.6}$$

where P_{ijkl}^I are the isospin projectors, $\mathcal{P}_J$ are the Legendre polynomials, and s_{VV} is the square of the centre-of-mass-energy for the VV system. More precisely, we work in the approximation of considering in the above expansion just the lowest partial wave amplitudes $I = 0, 1, 2$ and $J = 0, 1$; and we reconstruct the total amplitudes in terms of the unitarized partial wave amplitudes as given in sec.3 for the two different methods.

The differential cross-section in the Padé approximation is defined as:

$$(\frac{d\hat{\sigma}}{dcos\theta})^{[1,1]} = \frac{1}{64\pi M_{VV}^2}|T_{ijkl}^{[1,1]}|^2, \tag{4.7}$$

where

$$T_{ijkl}^{[1,1]} = 32\pi(a_{00}^{[1,1]}(s_{VV})P_{ijkl}^0 + a_{20}^{[1,1]}(s_{VV})P_{ijkl}^2 + 3cos\theta a_{11}^{[1,1]}(s_{VV})P_{ijkl}^1). \tag{4.8}$$

Similarly, the differential cross-section in the K-matrix approximation is defined as:

$$(\frac{d\hat{\sigma}}{dcos\theta})^K = \frac{1}{64\pi M_{VV}^2}|T_{ijkl}^K|^2, \tag{4.9}$$

where

$$T_{ijkl}^K = 32\pi(a_{00}^K(s_{VV})P_{ijkl}^0 + a_{20}^K(s_{VV})P_{ijkl}^2 + 3cos\theta a_{11}^K(s_{VV})P_{ijkl}^1). \tag{4.10}$$

The partial wave amplitudes $a_{IJ}^{[1,1]}$ and a_{IJ}^K of eqs. (4.8) and (4.10) are those of eqs. (3.9) and (3.6) respectively.

Finally, since we are interested in the processes with ZZ in the final state, the contribution of the two following subprocesses must be considered:

$$T(W_L^+ W_L^- \to Z_L^0 Z_L^0) \equiv T_{+-00}\ ;\ T(Z_L^0 Z_L^0 \to Z_L^0 Z_L^0) \equiv T_{0000}. \tag{4.11}$$

In that case, the isospin projectors appearing in eqs.(4.8) and (4.10) take the following numerical values:

$$P_{+-00}^0 = P_{0000}^0 = -P_{+-00}^2 = \frac{1}{3}\ ;\ P_{0000}^2 = \frac{2}{3}\ ;\ P_{+-00}^1 = P_{0000}^1 = 0. \tag{4.12}$$

5 Background processes

There are two background processes that are relevant for our study of strongly interacting signals with ZZ in the final state. These are:

$$pp \to (q\bar{q} \to Z^0 Z^0) + X$$

$$pp \to (gg \to Z^0 Z^0) + X.$$

The first process has been exhaustively studied in the literature, mainly in connection with the subject of heavy Higgs production at supercolliders (see for instance [24]). The cross-section for this process is given by:

$$\sigma = \sum_{i,j}\int\int d\tau d\eta\ f_i(x_1,Q^2)f_j(x_2,Q^2)\int_{-1}^{1} dcos\theta\frac{d\hat{\sigma}}{dcos\theta}(q\bar{q} \to Z^0 Z^0) \tag{5.1}$$

where we have used the same notation as in eq.(4.1), and:

$$\frac{d\hat{\sigma}}{dcos\theta}(q\bar{q} \to Z^0Z^0) = \frac{\pi\alpha^2\beta_Z}{192x_w^2(1-x_w)^2\hat{s}}(l_i^1 + r_i^1)[\frac{\hat{t}}{\hat{u}} + \frac{\hat{u}}{\hat{t}} + \frac{4M_Z^2\hat{s}}{\hat{u}\hat{t}} - M_Z^4(\frac{1}{\hat{t}^2} + \frac{1}{\hat{u}^2})] \quad (5.2)$$

with,

$$l_u = 1 - \frac{8}{3}x_w \; ; \; l_d = -1 + \frac{2}{3}x_w \; ; \; r_u = -\frac{8}{3}x_w \; ; \; r_d = \frac{2}{3}x_w. \quad (5.3)$$

The second process, taking place through a quark-loop, has been studied previously also in connection with heavy Higgs physics at supercolliders. Recently, it was computed analytically by the authors in ref.[25] who found that the gluon process can give a quite important contribution to ZZ production. In particular for the case of interest here (corresponding to ignoring the Higgs-quark triangle diagram in their computation), the cross-section for the gluon-gluon process as compared to the quark-antiquark process can be (at small invariant masses) as large as $60 - 70\%$ at the SSC and $35 - 40\%$ at the LHC.

In order to compute numerically the gluon-gluon background contribution we have implemented in our programs the analytical formulas of ref.[25] in the same way the authors do there. Following the same notation of eqs.(4.1) and (5.1), the cross-section is given by:

$$\sigma = \int\int d\tau d\eta \; g(x_1, Q^2)g(x_2, Q^2) \int_{-1}^{1} dcos\theta \frac{d\hat{\sigma}}{dcos\theta}(gg \to Z^0Z^0) \quad (5.4)$$

where the $g(x_{1,2}, Q^2)$ are the gluon distribution functions and

$$\frac{d\hat{\sigma}}{dcos\theta}(gg \to Z^0Z^0) = \frac{\alpha_s^2\alpha^2\beta_Z}{128^2\pi x_w^2(1-x_w)^2}(2\sum_H |\sum_q T_{qH}|^2). \quad (5.5)$$

Here, $\sum_H$ denotes the sum over all helicity states and $\sum_q T_{qH}$ indicates the sum over all the possible quarks flowing in the quark-loop for a given fixed helicity state H. For brevity, we do not write down here the expressions for the helicity amplitudes T_{qH}, but refer the reader to ref.[25], where the analytical formulas for both light quarks (q=u,d,s,c,b) and a heavy top quark can be found.

6 Numerical results

In this section we will present the numerical results for the signal and background processes and for the two planned pp-supercolliders, SSC and LHC. We take the following parameters:

$$SSC: \; \sqrt{s} = 40TeV \; ; \; \mathcal{L} = 10^{33}cm^{-2}sec^{-1}$$
$$LHC: \; \sqrt{s} = 16TeV \; ; \; \mathcal{L} = 4 \times 10^{33}cm^{-2}sec^{-1}$$

and will assume a total running time of :

$$\frac{1}{3}year \simeq 10^7 sec.$$

The assignment for the numerical values of the parameters appearing in our formulas has been done as follows:

I.- $m_u = 5.6MeV$, $m_d = 9.9MeV$, $m_s = 199MeV$, $m_c = 1.3GeV$, $m_b = 5GeV$;
$m_t = 100GeV$ and $180GeV$;
$M_W = 80GeV$, $M_Z = 91.1GeV$, $sin^2\theta_w = 1 - \frac{M_W^2}{M_Z^2}$;
$\alpha^{-1} = \alpha^{-1}(M_W^2) = 128$, $\alpha_s = \alpha_s(Q^2) = \frac{12\pi}{23}\frac{1}{log(\frac{Q^2}{\Lambda^2})}$, $\Lambda = 290MeV$.

II.- The structure functions of quarks and gluons are those of ELLIQ [24] ,set 2, with $\Lambda = 290MeV$. We have not taken into account the contribution of the top quark to the "sea" of the proton that for the top mass values considered here is negligible. The assignment for Q^2 in the distribution functions is:
$Q^2 = \hat{s}$ for $q\bar{q} \to Z^0Z^0$ and $gg \to Z^0Z^0$ (also in $\alpha_s(Q^2)$);
$Q^2 = M_W^2$ for $V_1V_2 \to V_3V_4$.

III.- For the QCD-like model we take:
$M_R(\nu) = M_R(0.785\frac{\nu}{f_s}GeV) - \frac{1}{12(4\pi)^2}log(\frac{\nu}{0.785\frac{\nu}{f_s}})$
$N_R(\nu) = N_R(0.785\frac{\nu}{f_s}GeV) - \frac{1}{6(4\pi)^2}log(\frac{\nu}{0.785\frac{\nu}{f_s}})$
where
$M_R(0.785\frac{\nu}{f_s}GeV) = -0.0009$; $N_R(0.785\frac{\nu}{f_s}GeV) = 0.0018$.
For the Higgs-like model we take:
$M_R(\nu) = \frac{1}{8}(c_1 - \frac{c_2}{2}) - \frac{1}{12(8\pi)^2}log(\frac{\nu}{M_H})$
$N_R(\nu) = \frac{c_2}{8} - \frac{1}{6(4\pi)^2}log(\frac{\nu}{M_H})$
where c_1 and c_2 are defined in eq.(2.11), and we have chosen $M_H = 20TeV$ so that the Padé approximation develops a scalar resonance at about $M_S \sim 1TeV$. Higher values of M_H would provide smaller values of M_S that we do not consider in this paper. In this case the expected rates are of the same order of magnitude as the corresponding ones, already studied in the literature, for a standard Higgs particle with the same mass. Lower values of M_H (but not too low, say, $M_H > 5TeV$) would provide lower rates than the ones presented in this paper for the Padé method, but they would be somehow close to the results given here for the K-matrix method. The scale ν in the definition of $M_R(\nu)$ and $N_R(\nu)$ for both models has been set ,for definiteness, to the value $\nu = 1TeV$, the results not being dependent on this choice.

The results are presented in the form of a total number of ZZ events (tables 1 and 2; 1.a and 2.a is for LHC, 1.b and 2.b is for SSC) , signal versus background, for a given set of cuts on the relevant kinematic variables: invariant mass of the ZZ pair, M_{ZZ}, transverse momentum of the final Z gauge bosons, p_{TZ}, and rapidity of the final $Z's$, $y_{1,2}$. The results are also given in the form of event-distribution with the variables M_{ZZ} and p_{TZ} (figs.3 and 4 respectively). The general cuts, being applied in all the numerical estimates, are the following (these will be referred to as "minimal cuts"):

$$0.5\,TeV \; < \; M_{ZZ} \; < \; 10TeV \; ; \; |p_{TZ}| \; > \; 10GeV$$

$$|y_{1,2}| \; < \; 1.5 \; (case \; A), \; |y_{1,2}| \; < \; 2.5 \; (case \; B).$$

The tables 1.a (LHC) and 1.b (SSC) show the resulting rates for the background and the signal after applying the minimal cuts. The various contributions coming from the different subprocesses: $W^+W^- \to Z^0Z^0$, $Z^0Z^0 \to Z^0Z^0$, $gg \to Z^0Z^0$ and $q\bar{q} \to Z^0Z^0$ are shown separately. The results for $gg \to Z^0Z^0$ corresponding to the two different choices of $m_t = 100GeV$ and $m_t = 180GeV$ are also included for comparison. The total rate for the signal is the sum of $W^+W^- \to Z^0Z^0$ and $Z^0Z^0 \to Z^0Z^0$. The total rate for the background is the sum of $q\bar{q} \to Z^0Z^0$ and $gg \to Z^0Z^0$. The upper half parts of the tables correspond to the predictions from the Padé unitarization method, and the lower half parts correspond to the predictions from the K-matrix unitarization method. The corresponding rates for the two models under investigation, the Higgs-like and the QCD-like models, are displayed with the short names Higgs and QCD respectively.

By looking at tables 1.a and 1.b we can make the following general remarks:

- Background:
  When comparing $gg \to Z^0Z^0$ versus $q\bar{q} \to Z^0Z^0$ we confirm the results of ref.[25]. That is, the gg fusion background is important but never dominant with respect to the $q\bar{q}$ background. The rates for gg versus $q\bar{q}$ being (case A):
  30%(10%) for $m_t = 100GeV$ ($m_t = 180GeV$) at LHC, and,
  57%(78%) for $m_t = 100GeV$ ($m_t = 180GeV$) at SSC.

- Dependence on the top mass:
  When comparing the gg fusion contribution for $m_t = 100GeV$ versus $m_t = 180GeV$ we always get higher rates for the heavier case. This is so because of the stringent cut given in M_{ZZ} of $M_{ZZ} > 500GeV$. Their distribution curves in M_{ZZ} cross at about $M_{ZZ} = 500GeV$ and for larger values of M_{ZZ} the curve for $m_t = 180GeV$ lies always above the $m_t = 100GeV$ one. This fact implies that the heavier the quark top is the more dangerous the gg background is for the search of strongly interacting signals.

- Efficiency of the rapidity cut:
  When going from $|y_{1,2}| < 2.5$ to $|y_{1,2}| < 1.5$ the rates for the signal and background are reduced to the following percentages of their original values:
  67% for the signal and 31% for the background at LHC, and
  60% for the signal and 32% for the background at SSC.

- Higgs-like model versus QCD-like model:
  When comparing the signal rates for the Higgs-like model to the ones for the QCD-like model, we learn that the Higgs/QCD ratio for both LHC and SSC is approximately the same, as well as for both choices of the rapidity cut. This ratio is always favourable to the Higgs-like model and is given by:
  2/1 for the Padé-unitarization method, and
  1.5/1 for the K-matrix-unitarization method.
  The fact that the rates for the Higgs-like model are always larger than the ones for the QCD-like model is simply because in the lowest partial wave approximation, the channels under investigation, $W^+W^- \to Z^0Z^0$ and $Z^0Z^0 \to Z^0Z^0$, are pure s-wave,

and the dominant contributing partial wave amplitude, a_{00}, is always larger in the Higgs-like case. Besides, the slight difference between the Padé and the K-matrix ratios is the reflection of $a_{00}^{[1,1]}$ being resonant in the Higgs-like model, in contrast to the non-resonant character of a_{00}^{K}.

- Total rates, signal versus background:
  If just the minimal cuts are applied the signal-to-background ratio is too small to be significant. For instance, in the most favourable case, i.e., for the Higgs-like model with $|y_{1,2}| < 1.5$ and $m_t = 100GeV$, we get a signal-to-background ratio of:
  1/7 for LHC, and, 2/7 for SSC.

In order to improve the signal-to-background ratio we have imposed additional cuts on M_{ZZ} and p_{TZ}. These cuts were not chosen arbitrarily but instead they were obtained by an optimization procedure as described in what follows. For a given pair of arbitrary cuts (p_{TZ}^c, M_{ZZ}^c) belonging to the parameter space ($p_{TZ} > 10GeV$, $M_{ZZ} > 500GeV$) we compute the total number of events with p_{TZ} and M_{ZZ} such that $p_{TZ} > p_{TZ}^c$ and $M_{ZZ} > M_{ZZ}^c$. We do it separately for the signal, $n_s(p_{TZ} > p_{TZ}^c, M_{ZZ} > M_{ZZ}^c)$, and the background, $n_b(p_{TZ} > p_{TZ}^c, M_{ZZ} > M_{ZZ}^c)$. We next define a function of p_{TZ}^c and M_{ZZ}^c as

$$F(p_{TZ}^c, M_{ZZ}^c) = \frac{n_s(p_{TZ} > p_{TZ}^c, M_{ZZ} > M_{ZZ}^c)}{[n_s(p_{TZ} > p_{TZ}^c, M_{ZZ} > M_{ZZ}^c) + n_b(p_{TZ} > p_{TZ}^c, M_{ZZ} > M_{ZZ}^c)]^{\frac{1}{2}}}, \qquad (6.1)$$

and we evaluate it at different possible choices for (p_{TZ}^c, M_{ZZ}^c) as obtained by scanning into the parameter space by small sequential bins $(\Delta p_{TZ}, \Delta M_{ZZ})$. The most appropriate cuts, called here optimal cuts, (p_{TZ}^0, M_{ZZ}^0), are then defined as the couple of cuts that maximize the function $F(p_{TZ}^c, M_{ZZ}^c)$, or, in other words, that maximize the statistical significance of the effect we are looking for.

The results after applying the optimal cuts are collected in tables 2.a (LHC) and 2.b (SSC) under the title "Optimal cuts" for the same various cases as in tables 1.a and 1.b, together with the couple of optimal cuts found for each case . The numbers shown in the tables correspond to the signal-to-background ratios for ZZ events and are written in the form: signal/background. For the columns entitled "Optimal cuts" the corresponding numbers of ZZ events are those placed in the first line of each box. The results for the rates obtained after applying just the minimal cuts are also included, for comparison, in tables 2.a an 2.b, under the title "Minimal cuts". Both values of m_t, $100GeV$ and $180GeV$, are considered.

In figs. 3 and 4 we have plotted the distribution of the events in the variables M_{ZZ} and p_{TZ} respectively (the figures shown are for $|y_{1,2}| < 2.5$). Figs. 3.a and 4.a correspond to the predictions from the Padé method and figs. 3.b and 4.b are the ones from the K-matrix method. In all the figures the two upper histograms are the predictions for LHC, and the two lower histograms are the results for SSC. Solid lines are the total rates, signal plus background. Dashed lines are just the background rates.

Apart from the general comments made before for the results with just the minimal cuts that still hold now for the new results , we find that with the optimal cuts there is a remarkable improvement in the signal-to-background ratio for both colliders LHC and SSC. For instance, at LHC with $|y_{1,2}| < 2.5$ and $m_t = 180GeV$, after applying the optimal cuts, the signal is just reduced to $50 - 60\%$ of its original value whereas the background is reduced to less than 10%. The corresponding numbers for SSC are $60 - 70\%$ for the signal and less than 20% for the background.

Finally, in order to estimate how statistically significant is the obtained enhancement in the total number of ZZ events, we conservatively assume that it will be possible to identify as true ZZ events only those containing four leptons, the so-called gold-plated events, $l^+l^-l^+l^-$ with $l = e$ or μ. This choice will provide the most conservative rates since it reduces the ZZ rate events by a very small branching ratio of $BR(ZZ \to l^+l^-l^+l^-) = \frac{1}{3} \times 1 \times (0.033)^2 = 1.5 \times 10^{-3}$. However, this choice has the advantage of providing the safest predictions as far as experimental detection is concerned.

The resulting rates for the gold-plated events are collected in the columns entitled "Optimal cuts" of tables 2.a (LHC) and 2.b (SSC) just below the ZZ events rates, together with the value found for the optimal cuts. They are also shown in the form of signal/background. As can be seen from these numbers, with the optimal cuts the signal-to-background ratio improves very much for both colliders LHC and SSC, with a slightly better improvement in the SSC case which for some of the various situations studied in this paper gives a signal-to-background ratio close to one (see for instance in table 2.b the Higgs-like model with $|y_{1,2}| < 1.5$ and $m_t = 100GeV$). However, this is not the whole story, since it turns out that whereas in the LHC the signal-to-background ratio is statistically significant for several situations among the ones considered in table 2.a, it is certainly not the case for the SSC (except for the Higgs-like model with $|y_{1,2}| < 2.5$ and $m_t = 100GeV$ that may have some chance).

The statistical significance of the excess of $l^+l^-l^+l^-$ events over the background coming from the strongly interacting LWB processes may be estimated by means of the function $F(p_{TZ}^0, M_{ZZ}^0)$ of eq.(6.1) evaluated at the optimal cuts as follows:

$$N = F(p_{TZ}^0, M_{ZZ}^0) \times \sqrt{BR(ZZ \to l^+l^-l^+l^-)}.$$

Here, N gives the number of $\sigma's$ associated to the expected effect of enhancement in the number of $l^+l^-l^+l^-$ events due to the strongly interacting LWB processes. We find at SSC a numerical value for N always less than one (except for the Higgs-like model case with $|y_{1,2}| < 2.5$ and $m_t = 100GeV$ that gives $N \sim 1$), whereas at LHC one gets in general much more promising values. For instance, the predictions from the Padé approximation give a statistical significance as large as $N \sim 2$ for the Higgs-like model, and $N \sim 1$ for the QCD-like model.

We believe that the numerical results presented in this paper are a clear indication of the new open possibilities for the LHC machine with the high luminosity option in what

concerns the search of strongly interacting LWB signals.

7 Conclusions

We have shown that by applying a simple model for the scattering amplitudes of strongly interacting LWB, based on the well-known techniques from chiral effective Lagrangians and ChPT, supplemented by some unitarization method, one can make reasonable estimates of the signal rates at pp supercolliders like the future machines SSC and LHC. The method allows us to distinguish between different models for the underlying unknown dynamics governing the symmetry breaking sector of the SM.

The numerical results presented in this work show that both SSC and LHC will provide a considerable enhancement in the number of ZZ events if the symmetry breaking sector of the SM is strongly interacting. In particular, if the planned high luminosity option for the LHC is assumed to be reached, the signal-to-background ratio for this machine is found to be quite promising, even in the most pessimistic case of considering just the $l^+l^-l^+l^-$ gold-plated events. For the SSC, however, after applying our set of optimal cuts, we do not find enough $l^+l^-l^+l^-$ events left to be statistically significant. Hence, at the SSC, in order to study the strongly interacting LWB signals one is forced to look at different channels from the gold-plated events, for instance hadronic channels and $l^+l^-\nu\bar{\nu}$ channels. We do not consider these in this paper.

Acknowledgements

We would like to thank Maria Teresa Urdiales for her valuable participation in the computation of the cross-section for the $q\bar{q}$ background process. J.T. is grateful to E.Glover for some clarifying comments on the gluon-gluon helicity amplitudes. A.D. is indebted to the "Escuela de Postgrado y Especializacion", CSIC (Spain) for financial support.

References

[1] J.M. Cornwall,D. N. Levin and G. Tiktopoulos, Phys. Rev. **D10** (1974)1145.
B. W. Lee, C. Quigg and H. Thacker, Phys. Rev. **D16**(1977)1519.
M. Veltman, Acta Phys. Pol. **B8**(1977)475.
M. S. Chanowitz and M. K. Gaillard, Nucl. Phys. **B261**(1985)379.

[2] Gauge boson fusion in pp colliders was first discussed in:
R.N.Cahn and S.Dawson, Phys.Lett.**136B**(1984)196; **138B**(E)(1984)464.
For recent studies see:
R.N.Cahn et al. in *Proceedings of the Workshop on Experiments, Detectors, and Experimental Areas for the Supercollider*. Ed. by R.Donaldson and M.Gilchriese, World Scientific, Singapore, 1988,p.20.
D.Froidevaux et al. in *Proceedings of the Workshop on Physics at Future Accelerators*. Ed. by J.Mulvey. CERN preprint, CERN/87-07 (1987).

[3] M. Chanowitz, M. Golden and H. Georgi, Phys. Rev. **D36**(1987)1490.

[4] For a recent review of the field and many further references, see
M. S. Chanowitz, Ann. Rev. Nucl. Part. Sci. **38**(1988)323.

[5] S.Weinberg, Phys.Rev.Lett. **17**(1966)11.

[6] A.Dobado and M.J. Herrero, Phys.Lett.**B228**(1989)195; **B233**(1989)505.

[7] A similar philosophy has been followed recently also in:
J.F.Donoghue and C.Ramirez, Phys.Lett.**B234**(1990)361.

[8] Report of the Scientific Policy committee, 157th meeting, *The Large Hadron Collider Project*. CERN preprint, CERN/SPC/582, Sept.1989.

[9] U. Amaldi et al., Phys.Rev.**D36**(1987)1385.

[10] S. Weinberg, Physica **96 A**(1979)327.

[11] J. Gasser and H. Leutwyler, Ann. of Phys. **158**(1984)142.

[12] H.Georgi, *Weak Interactions and Modern Particle Theory*, Benjamin-Cummings,1984.

[13] S. Dawson and S. Willenbrock, Phys. Rev. Lett. **62** (1989)1232; Brookhaven National Laboratory Preprint, BNL-42767, May(1989).

[14] M.Veltman and F.J.Yndurain, Univ. of Michigan Preprint, UM-TH-89-04, March(1989).

[15] A.Dobado, M.J.Herrero and T.N.Truong, Phys.Lett.**B235** (1990)129.
A.Dobado, CERN preprint, CERN-TH.5572/89, to appear in Phys.Lett.B.

[16] J. F. Donoghue, C. Ramirez and G. Valencia, Phys. Rev. **D38** (1988)2195.

[17] A.Dobado, M.J.Herrero and T.N.Truong, Phys.Lett.**B235** (1990)131.

[18] J.L.Basdevant, Fortsch.Phys.**20**(1972)283.

[19] S.N.Gupta, *Quantum Electrodynamics*, Ed. by Gordon and Breach, New York (1981)191.

[20] O.Cheyette and M.K.Gaillard, Phys.Lett.**B197**(1987)205.

[21] D.A.Dicus and W.Repko, Phys. Lett.**B228**(1989)503.

[22] CDF collaboration, F.Abe et al., UPR-0172E, submitted to Phys. Rev.Lett.

[23] S. Dawson, Nucl. Phys. **B249**(1985)42.

[24] E.Eichten et al., Rev.Mod.Phys.**56**(1984)579.

[25] E.W.N.Glover and J.J.Van der Bij, Nucl.Phys.**B321**(1989)561.

Figure Captions

Fig. 1: Schematic representation of the $V_L - V_L$ fusion process for testing strongly interacting LWB at proton-proton supercolliders.

Fig. 2: Behaviour with energy of the partial wave amplitudes for the different approaches and models considered in this paper. Solid lines are the predictions from ChPT before unitarization, i.e., eq.(3.1). Dotted lines are the ones after unitarization with the Padé method, eq.(3.9), and dashed lines with the K-matrix method, eq.(3.6). The curves in (a),(b) and (c) correspond to $M_H = 20, 10, 5TeV$ respectively. Plots (d), (e) and (f) are for $M_H = 20TeV$.

Fig. 3: ZZ-events distribution (per bin of $50GeV$) with respect to the invariant mass $M_{ZZ}(GeV)$ for the various approches and models explained in the text. The two upper histograms in each one of the plots are for LHC and the two lower ones are for SSC. Solid histograms are the total rates, signal plus background. Dashed histograms are the background contribution alone. Histograms in (a) are the predictions from the Padé unitarization method. Histograms in (b) are from the K-matrix method. The two windows of the plots (a) and (b) placed to the left correspond to the Higgs-like model. The ones to the right are the predictions for the QCD-like model.

Fig. 4: ZZ-events distribution (per bin of $60GeV$) with respect to the transverse momentum of the $Z's$ in the final state $p_{TZ}(GeV)$. The notation in figs.(a) and (b) is the same as in figs.3.a and 3.b.

Table Captions

Table 1: (a) ZZ-events rates at LHC with just the minimal cuts for the various channels contributing to the strongly interacting LWB signals and to the background. Case A is for $|y_{l,2}| < 1.5$. Case B is for $|y_{l,2}| < 2.5$.
(b) Same for SSC.

Table 2: (a) ZZ-events rates at LHC for the signal/background after applying the optimal cuts as described in the text. The corresponding $l^+l^-l^+l^-$ events rates for the signal/background are also included together with the numerical values for the optimal cuts. Case A is for $|y_{l,2}| < 1.5$. Case B is for $|y_{l,2}| < 2.5$.
(b) Same for SSC.

	LHC 16 TeV	$W^+W^- \to Z^0Z^0$	$Z^0Z^0 \to Z^0Z^0$	$gg \to Z^0Z^0$ $m_t = 100GeV$	$gg \to Z^0Z^0$ $m_t = 180GeV$	$q\bar{q} \to Z^0Z^0$	Total Signal	Total Backg. $m_t = 100GeV$	Total Backg. $m_t = 180GeV$
Pade	Higgs (A)	7308	1782	14295	18281	49242	9090	63537	67523
	QCD (A)	3963	337				4300		
	Higgs (B)	10980	2580	29125	34497	173825	13560	202950	208322
	QCD (B)	5938	476				6414		
K-Matrix	Higgs (A)	4385	954	14295	18281	49242	5339	63537	67523
	QCD (A)	3457	318				3775		
	Higgs (B)	6600	1346	29125	34497	173825	7946	202950	208322
	QCD (B)	5202	448				5650		

Table 1.a

	SSC 40 TeV	$W^+W^- \to Z^0Z^0$	$Z^0Z^0 \to Z^0Z^0$	$gg \to Z^0Z^0$ $m_t = 100GeV$	$gg \to Z^0Z^0$ $m_t = 180GeV$	$q\bar{q} \to Z^0Z^0$	Total Signal	Total Backg. $m_t = 100GeV$	Total Backg. $m_t = 180GeV$
Pade	Higgs (A)	1164	333	1917	2600	3346	1497	5263	5946
	QCD (A)	669	79				748		
	Higgs (B)	1988	552	4280	5358	12347	2540	16627	17705
	QCD (B)	1129	126				1255		
K-Matrix	Higgs (A)	707	237	1917	2600	3346	944	5263	5946
	QCD (A)	565	81				646		
	Higgs (B)	1201	375	4280	5358	12347	1576	16627	17705
	QCD (B)	958	127				1085		

Table 1.b

	LHC 16 TeV	Minimal Cuts $m_t = 100GeV$	Optimal Cuts $m_t = 100GeV$ $(p_{t_\tau}^0(GeV), M_{ZZ}^0(GeV))$	Minimal Cuts $m_t = 180GeV$	Optimal Cuts $m_t = 180GeV$ $(p_{t_\tau}^0(GeV), M_{ZZ}^0(GeV))$
Pade	Higgs (A)	9090 / 63537	5939 / 10766 9 / 16 (300,750)	9090 / 67523	5939 / 12913 9 / 19 (300,750)
	QCD (A)	4300 / 63537	2145 / 8079 3 / 12 (360,750)	4300 / 67523	2635 / 15333 4 / 23 (300,700)
	Higgs (B)	13560 / 202950	7553 / 16979 11 / 25 (300,750)	13560 / 208322	8397 / 25001 13 / 37 (240,750)
	QCD (B)	6414 / 202950	3352 / 19905 5 / 30 (300,700)	6414 / 208322	3352 / 22985 5 / 34 (300,700)
K-Matrix	Higgs (A)	5339 / 63537	3124 / 10766 5 / 16 (300,750)	5339 / 67523	3124 / 12943 5 / 19 (300,750)
	QCD (A)	3775 / 63537	2217 / 12894 3 / 19 (300,700)	3775 / 67523	2217 / 15333 3 / 23 (300,700)
	Higgs (B)	7946 / 202950	4282 / 19905 7 / 30 (300,700)	7946 / 208322	4282 / 22985 7 / 35 (300,700)
	QCD (B)	5650 / 202950	2813 / 19905 4 / 30 (300,700)	5650 / 208322	3040 / 26994 5 / 40 (300,600)

Table 2.a

	SSC 40 TeV	Minimal Cuts $m_t = 100GeV$	Optimal Cuts $m_t = 100GeV$ $(p_{t_\tau}^0(GeV), M_{ZZ}^0(GeV))$	Minimal Cuts $m_t = 180GeV$	Optimal Cuts $m_t = 180GeV$ $(p_{t_\tau}^0(GeV), M_{ZZ}^0(GeV))$
Pade	Higgs (A)	1497 / 5263	1143 / 1261 2 / 2 (240,750)	1497 / 5946	1143 / 1715 2 / 3 (240,750)
	QCD (A)	748 / 5263	453 / 794 <1 / 1 (360,800)	748 / 5946	482 / 1340 <1 / 2 (300,800)
	Higgs (B)	2540 / 16627	1791 / 2484 3 / 4 (240,750)	2540 / 17705	1791 / 3178 3 / 5 (240,750)
	QCD (B)	1255 / 16627	658 / 1357 1 / 2 (360,800)	1255 / 17705	772 / 2668 1 / 4 (300,750)
K-Matrix	Higgs (A)	944 / 5263	587 / 794 <1 / 1 (360,800)	944 / 5946	663 / 1551 1 / 2 (300,750)
	QCD (A)	646 / 5263	374 / 794 <1 / 1 (360,800)	646 / 5946	426 / 1551 <1 / 2 (300,750)
	Higgs (B)	1576 / 16627	938 / 1739 2 / 3 (300,800)	1576 / 17705	993 / 2668 2 / 4 (300,750)
	QCD (B)	1085 / 16627	561 / 1480 <1 / 2 (360,700)	1085 / 17705	639 / 2668 1 / 4 (300,750)

Table 2.b

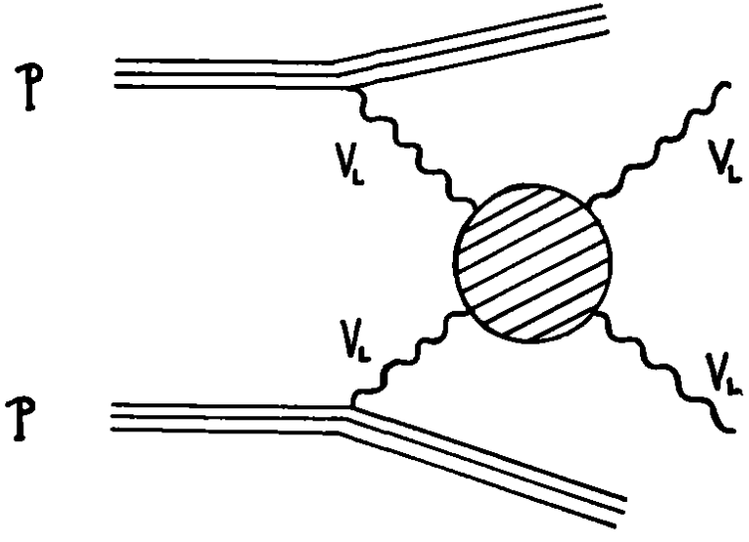

Figure 1

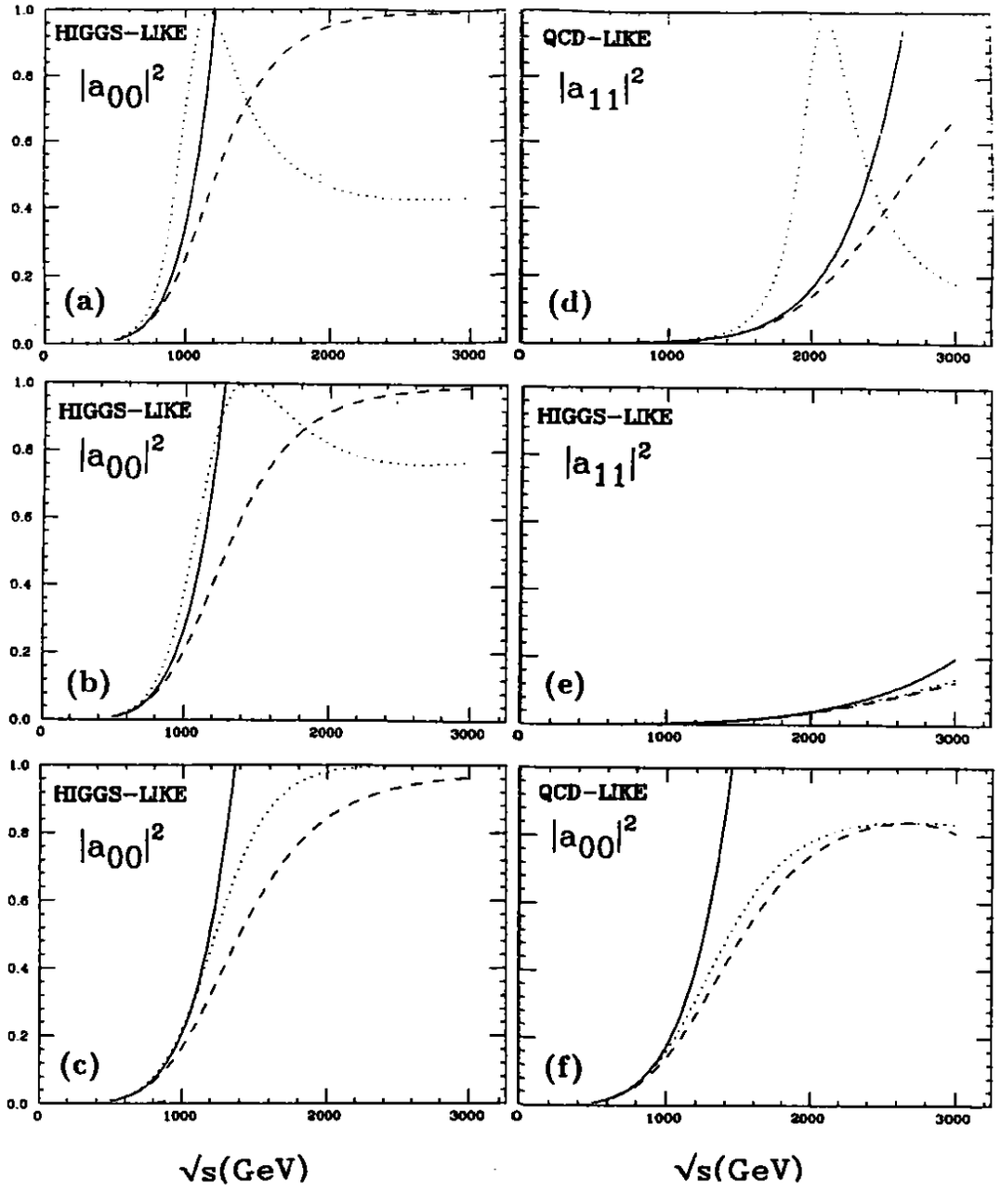

Figure 2

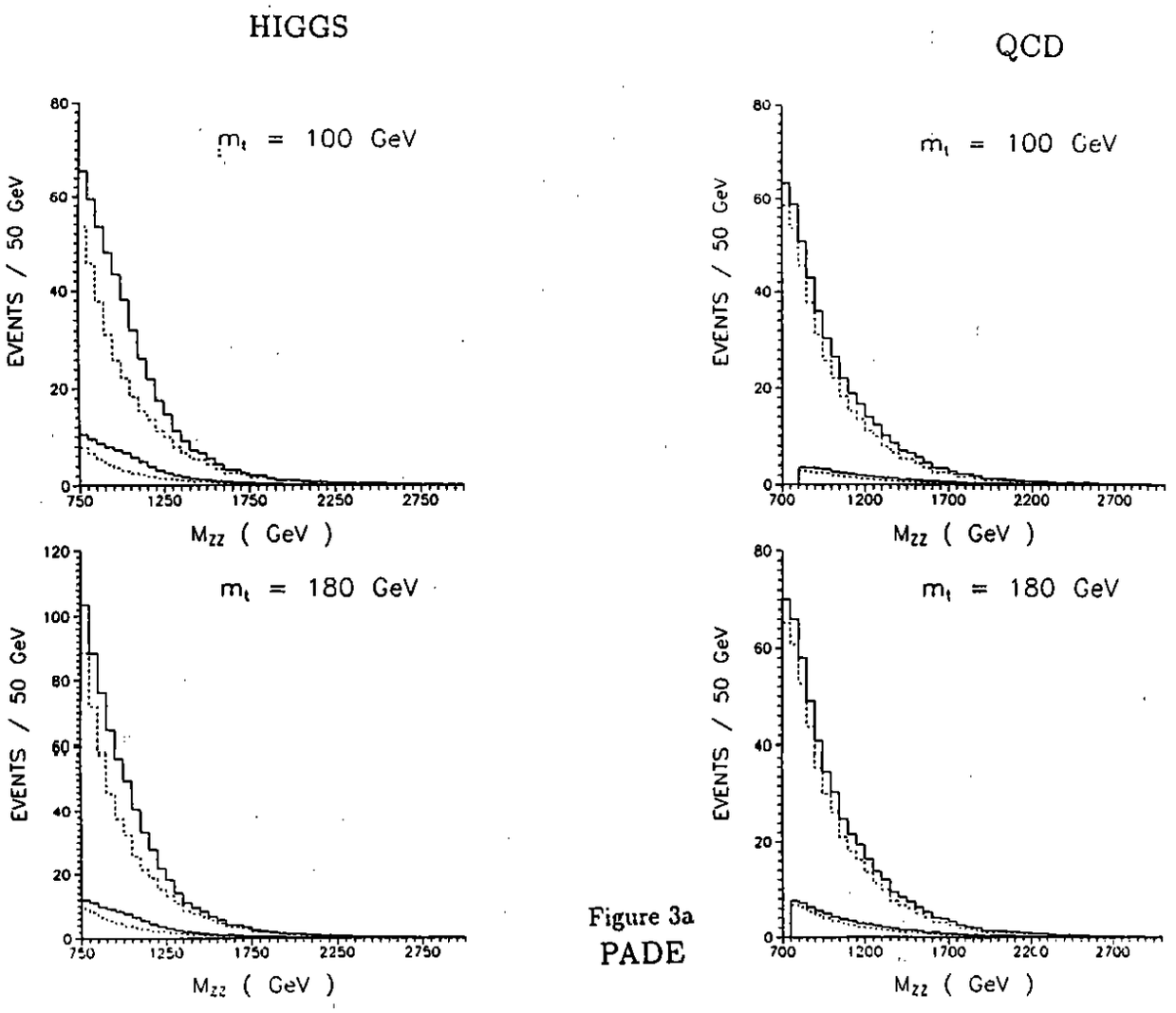

Figure 3a
PADE

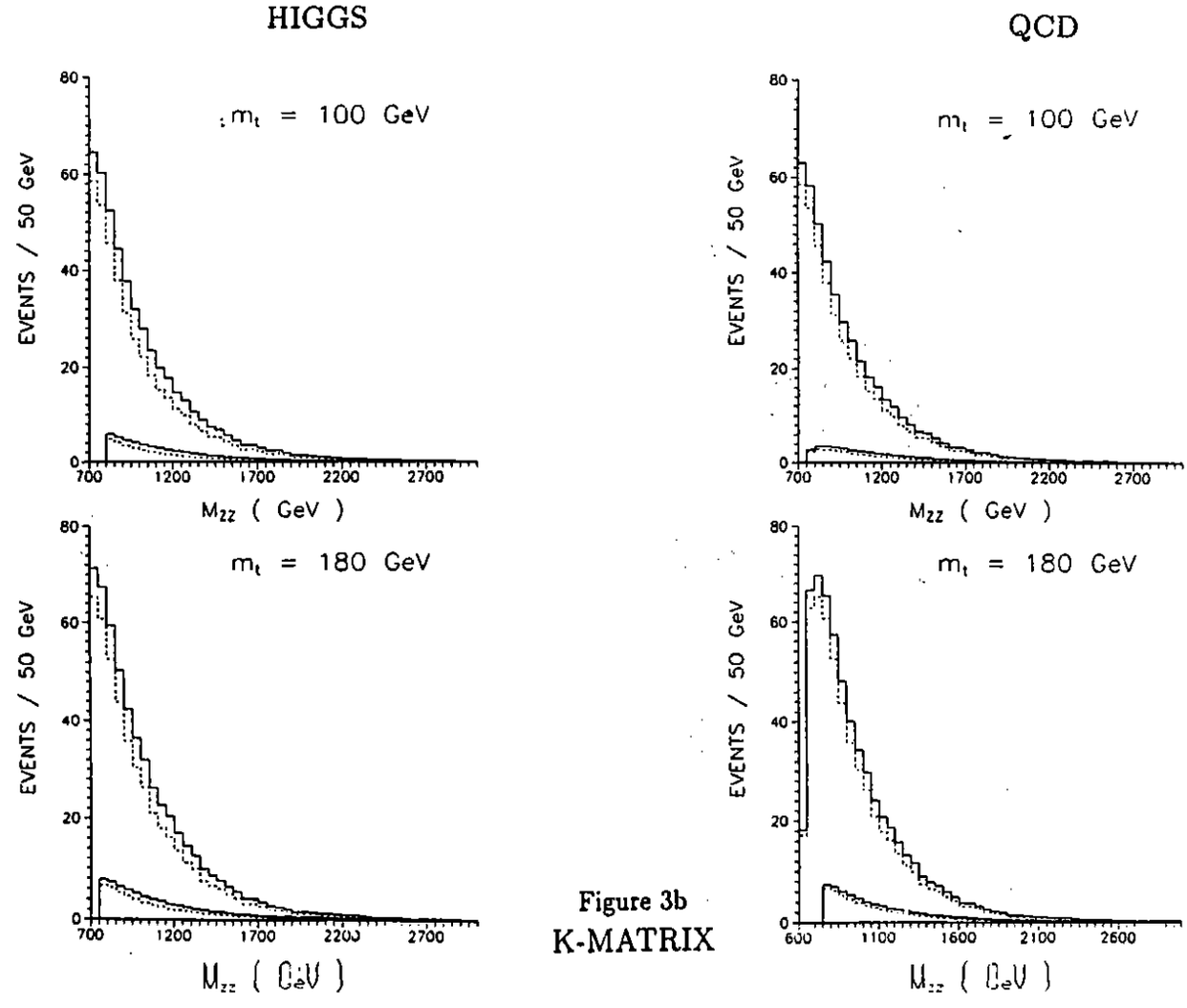

Figure 3b
K-MATRIX

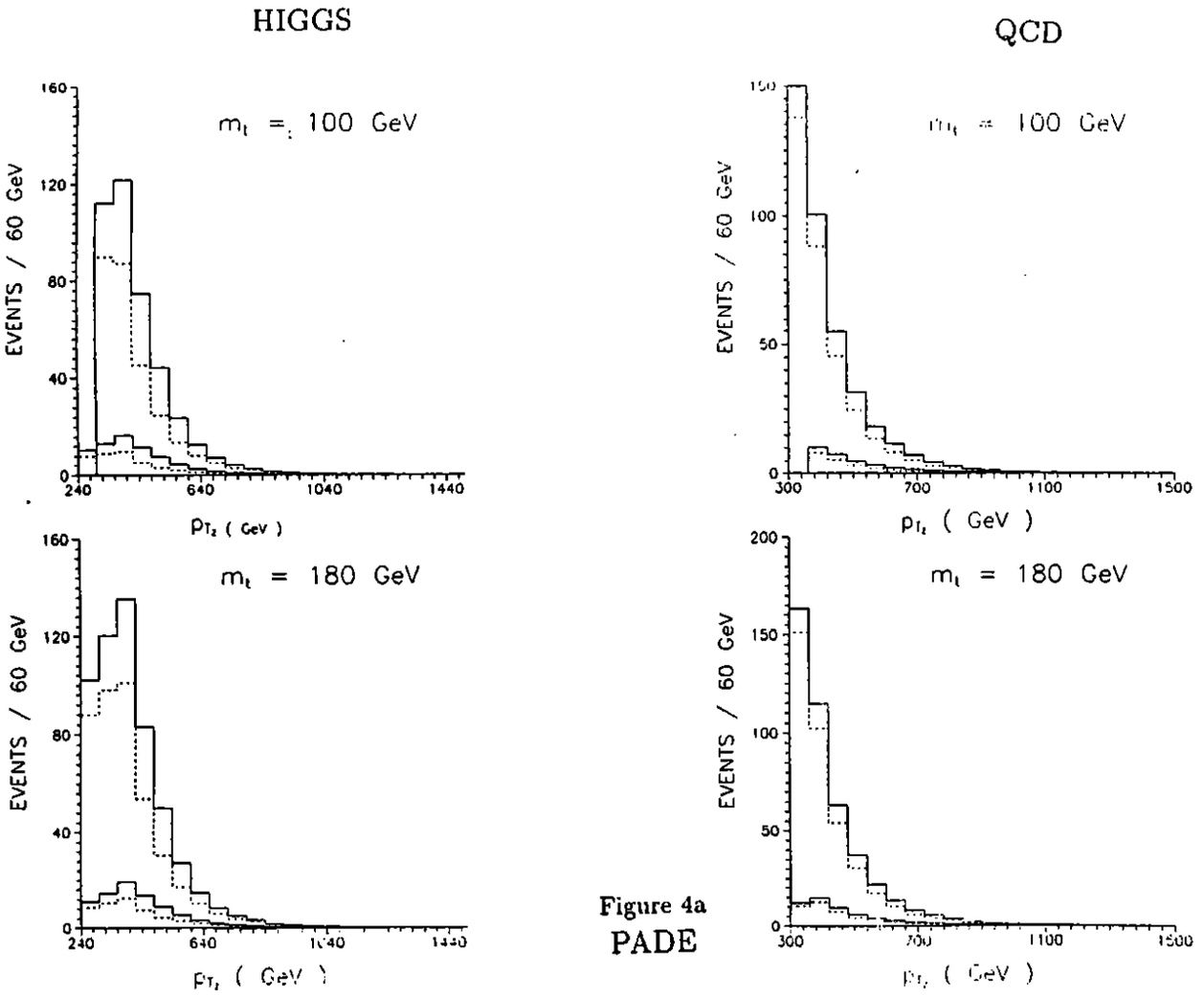

Figure 4a
PADE

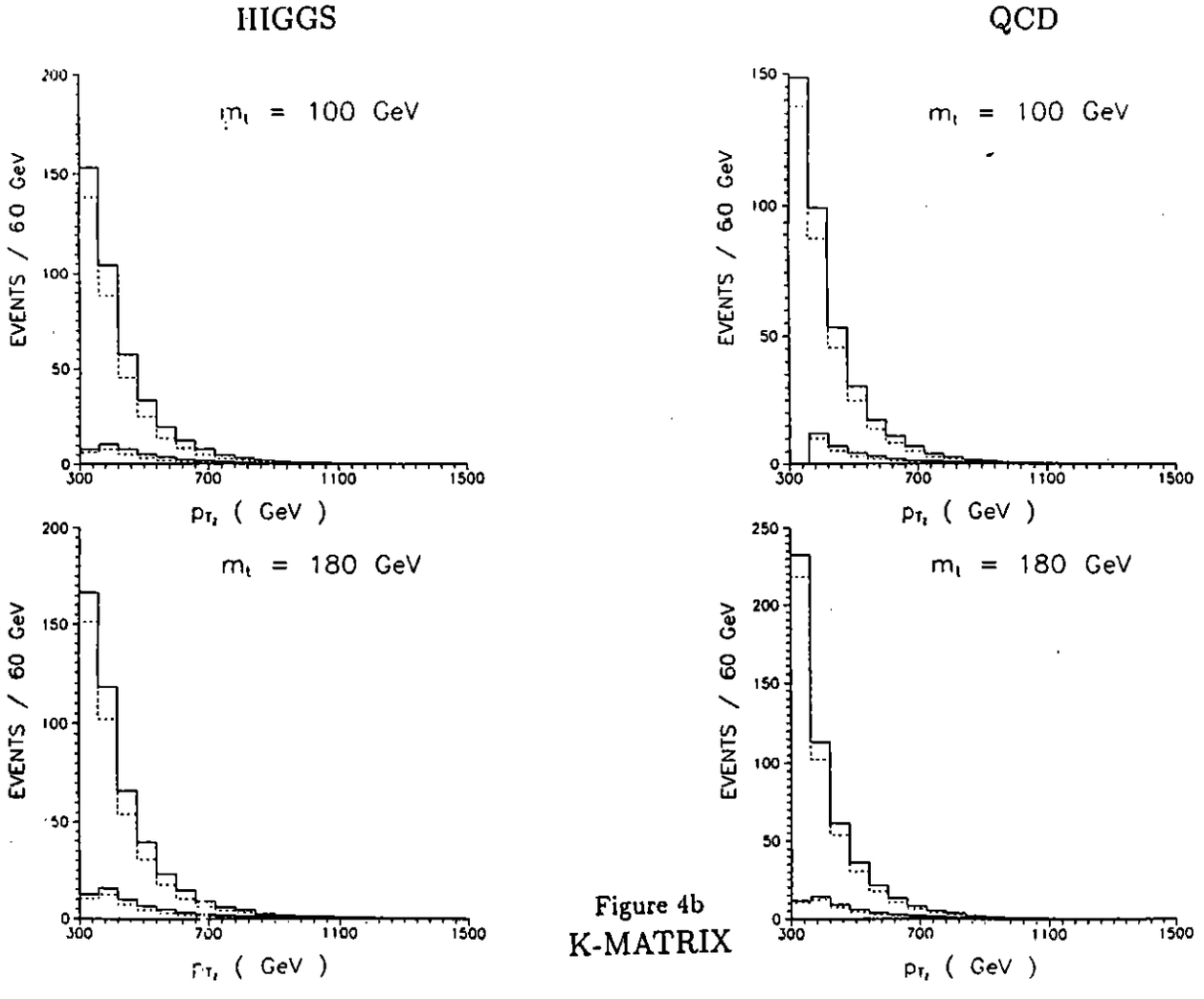

Figure 4b
K-MATRIX